THREE-DIMENSIONAL MEASUREMENTS OF FLOW AND SCALAR DISPERSION THROUGH A STADIUM USING MRI

Megan Colpo, Ty Homan, Zachary Zalar, Michael J. Benson, Andrew J. Banko
Civil & Mechanical Engineering
United States Military Academy
752 Thayer Rd, West Point, NY 10996
ty.homan@westpoint.edu

Christopher J. Elkins, John K. Eaton
Mechanical Engineering
Stanford University
488 Escondido Mall, Stanford, CA 94305
celkins@stanford.edu

ABSTRACT

A contaminant release within a stadium is studied experimentally using MRI techniques. The stadium geometry includes several realistic features, such as tunnels and a large roof opening, that enable ventilation and affect internal flow. MRI techniques are well suited for resolving flows in challenging internal geometries, and the three-dimensional measurements provide detailed insight into the complex flow and scalar dispersion occurring in, through, and around the stadium. Three-component velocity measurements were obtained for 0 and 45 degree wind angles measured relative to the minor axis of the roof opening. In both orientations, openings on the sides of the stadium provide most of the inflow, while the large roof opening provides most of the outflow. The data also demonstrate differences between the flow fields in the two orientations. Pressure gradients in the 0 degree orientation cause flow to enter the stadium via openings on its leeward side, while flow exits the stadium through openings on that side in the 45 degree case. The velocity results suggest that the 45 degree orientation yields a higher level of ventilation overall. Concentration measurements were obtained for the 0 degree wind angle, and demonstrate that recirculation causes contaminant to collect in the windward side of the stadium. Contaminant primarily exits the stadium through the roof, forming an elevated downstream plume. High concentrations within the stadium relative to the wake suggest that contaminant residence times within the stadium are significant. Along with providing detailed insight into ventilation dynamics, the MRI datasets are expected to be advantageous for robust model evaluation efforts.

INTRODUCTION

Prediction of flow and scalar dispersion within the built environment is relevant for structural design, air quality management, and threat response. However, computational fluid dynamics (CFD) models are challenged by the broad range of length scales inherent to urban areas, as the dynamic atmospheric boundary layer interacts with buildings and other objects to yield a complex flow field (Blocken, 2015). CFD simulations therefore require robust experimental datasets with well-posed boundary conditions to evaluate accuracy and inform model improvement.

While many experimental and computational studies have focused on external urban canopy flows (Britter and Hanna, 2003; Lateb et al., 2016), there have been fewer investigations involving flow through buildings or structures with porous features. Additional complexity is introduced in such scenarios, as openings and porous features enable interactions between internal and external flow. Van Hooff et al. conducted several computational studies related to flow and dispersion through a stadium, with the intent of providing insights related to ventilation (2010), pollutant exposure (2013), and more. The computational results were detailed; however, validation was performed using sparse experimental data and could be improved by comparing to full-field measurements.

Obtaining detailed experimental data is challenging for scenarios involving naturally ventilated buildings. Restrictive internal geometries can prevent the usage of techniques that are either intrusive or require optical access. Moreover, the large spatial variability inherent to internal-external flow interaction poses a challenge for the resolution of conventional measurement techniques. Most experimental studies related to building ventilation have been performed in wind tunnels with the aid of discrete probes (Ohba et al., 2001; Jiang et al., 2003). In-situ measurements have also been obtained at full scale, commonly employing pressure transducers or anemometers (Caciolo et al., 2011; Lo and Novoselac, 2012). Because these techniques are challenged by the small pressure differences associated with natural ventilation, other studies use tracer-gas methods as an indirect form of measurement (Remion et al., 2019). In general, the aforementioned studies are limited by the use of discrete measurement devices, which are typically intrusive and challenged to resolve complex flow.

A suite of experimental methods uses Magnetic Resonance Imaging (MRI) to non-optically and non-intrusively measure flow quantities for internal or external flow in arbitrarily complex geometries. Measurements are taken inside a water channel, allowing for the precise control of inlet and boundary conditions. Additionally, inlet conditions are directly measured as part of the resulting dataset. MRI methods yield full-field, three-component mean

velocity and concentration data at O(10^6) points over a three-dimensional domain (Benson et al., 2019). As such, MRI measurements provide new opportunities for model validation in challenging internal geometries. MRI techniques have been applied to scaled experiments involving both mock urban arrays (Shim et al., 2019; Owkes et al., 2020) and geometry related to the JU2003 tests (Benson et al., 2019; Homan et al., 2021), with demonstrated utility for CFD validation (Brown et al., 2020).

In the present study, MRI methods have been applied to the measurement of flow and dispersion in, through, and around a generalized stadium structure. The stadium geometry was inspired by Van Hooff et al. (2010) and has a roof structure with a rectangular open section, as well as four tunnels similar in design to what may be used for ingress and egress to seating areas. Velocity component measurements were obtained for two wind directions and concentration data were measured for one of the orientations. The measurements provide insight into ventilation and dispersion characteristics and should be useful for future validation efforts.

EXPERIMENTAL METHODS

An idealized stadium model (see Fig. 1-4) was designed as a 1:2060 representation of basic features of the Amsterdam Arena used by Van Hooff et al. (2010). The model also represents generic features from other stadiums (e.g, roof opening, multi-level seating, etc.). To minimize blockage in the channel, the height of the model was scaled to a height of 25 mm and an outside diameter of 92 mm. These dimensions were selected to ensure that a blockage ratio of 0.12 within the channel was met, while providing the capacity to create porous features that were realistic and could be captured by the resolution of the MRI measurements. The geometry features a partially open roof design with four entrances at ground level accessible via ramps. The 6 mm x 6 mm cross-section of each entrance accommodated nine voxels of data with a 1.2 mm scan resolution. Other key features allowed for at least one voxel in each plane. The stadium interior has two levels of seating around a circular event arena and four external sets of supports for a roof with a rectangular opening. Four openings, hereafter referred to as ventilation gaps, were added just below the roof to simulate retractable roof designs. These design decisions were chosen to mimic common stadium features and allow flow both through and around the stadium via multiple openings. At the base of the stadium is a flange connecting it to the bottom of the water channel section and which could be rotated to vary the wind angle by 22.5 degree increments. A passive scalar was released from an injector in the base of the stadium via of an array of 2.0 mm holes at the stadium floor fed by a plenum. The hole array was designed to inject contaminant at low velocity across the entire stadium so the effects of ventilation features could be directly observed.

The stadium was housed within a 2.2 m long water channel (see Fig. 5) that consists of three gridded diffuser sections and a contraction to increase flow uniformity. To develop a fully turbulent boundary layer, representative of neutrally stable conditions within an urban canopy, flow travels through an upstream section with a four-row cuboid building array with 14 mm x 14 mm bases. The cuboid sizing is similar to buildings surrounding a stadium, and the array is placed far enough upstream so that mean flow effects are minimized near the stadium. This distance was approximated using the results in Lien and Yee (2004). The array ends 160

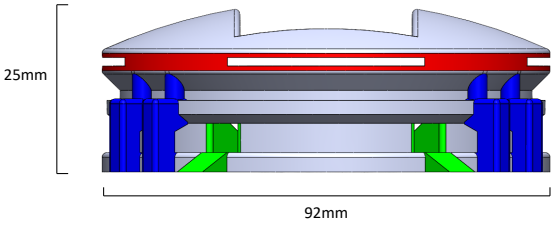

Figure 1. Side view of Stadium geometry showing generalized stadium features such as stadium entrances (green), open roof, roof slits (red), and roof supports (blue).

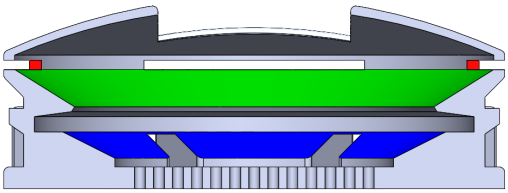

Figure 2. Side view section cut of stadium geometry showing two floor seating (blue and green) and roof slits (red).

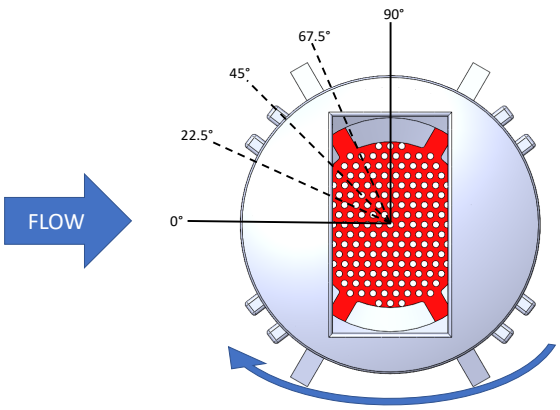

Figure 3. Top view of stadium geometry showing rotation and wind angles

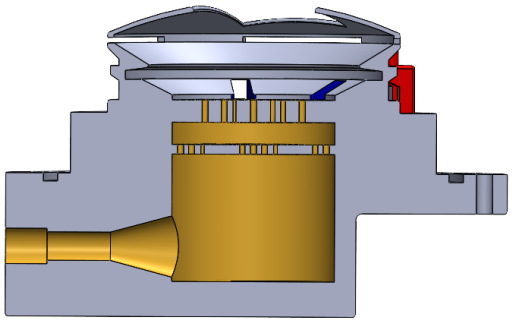

Figure 4. Side view of injector geometry showing inlet, plenum, and hole arrays.

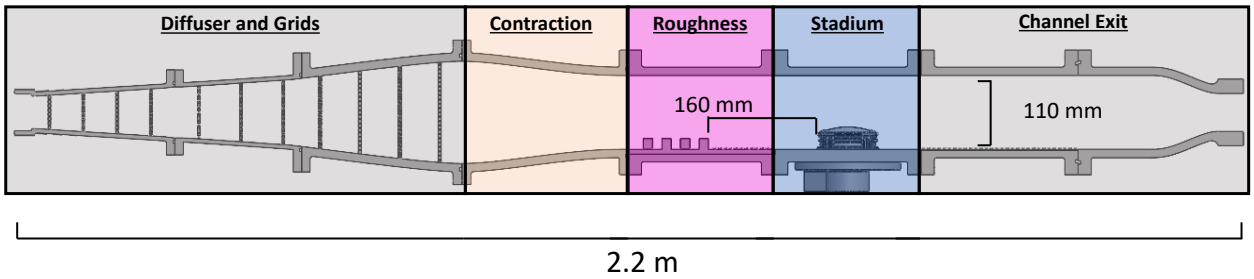

Figure 5. Section cut of water channel.

mm upstream of the stadium followed by a regular grid of short cylinders representing uniform roughness so that the building wakes recover prior to interacting with the stadium

Within the 110 mm by 196 mm main channel, the bulk velocity was 0.3 m/s, giving a Reynolds number of 10,500 based on the stadium height of 25 mm. For the stadium entrances, the Reynolds number is 290 based on the tunnel height and the measured velocity as described in Figure 8. Based on the cuboid the height and the bulk velocity, the cuboid Reynolds number was 4700. The velocity through the hole array in the stadium floor was 0.0485 m/s. As shown in Figure 4, the hole array covers the entire floor of the stadium to provide an evenly distributed contaminant injection that minimizes interference with the natural velocity profiles inside the stadium.

Magnetic resonance velocimetry (MRV) and magnetic resonance concentration (MRC) were used to measure the 3D mean velocity and concentration fields in and around the stadium. Both techniques utilized a GE Discovery MR750 3.0T Magnetic Resonance Imaging (MRI) system at the Richard M. Lucas Center at Stanford University. MRV used an aqueous solution of 0.06 M CuSO4 and a phase-contrast sequence as described in Elkins and Alley (2007) to acquire the 3D, 3-component mean velocity field on an isotropic Cartesian grid with 1.2 mm resolution. MRC was conducted at the same scan resolution and used a fast-spoiled gradient echo sequence (Banko et al., 2020). Three scan types are used to construct the concentration field: background scans using plain water for the main and injection flow, reference scans using 0.02 M CuSO4 solution for the main and injection flows, and standard scans using water for the main flow and 0.02 M CuSO4 solution for the injection flow. A second, higher concentration standard scan using 0.1 M CuSO4 solution was also incorporated to improve signal-to-noise ratio in low concentration regions of the plume. The concentration field is computed by background-subtracting the standard scans and then normalizing by the difference between reference and background scans, and therefore varies from unity in the injector to zero in the freestream (Banko et al., 2020). The resulting uncertainties were approximately 6% of the freestream velocity for MRV and 4% of the injected concentration for MRC.

RESULTS

Flow Field Analysis

Figure 6 provides an illustration of the key flow mechanisms and directions within the stadium at the centerplane. Flow within the stadium is complex and three-dimensional, generally following characteristics of driven cavity flow (Shankar and Deshpande, 2000). A large vortex dominates in the 0 degree orientation, causing flow to recirculate from the leeward side of the stadium cavity, across the floor, and finally vertically upwards at the windward side. Recirculation is also dominant in the 45 degree orientation, especially under the large roof overhangs.

The streamwise velocity fields for both the 0 and 45 degree stadium orientations are represented in Figure 7 with contour planes located at two heights. As demonstrated by the contours, the stadium creates an obstruction within the flow field that causes mainstream flow to accelerate. Freestream velocity increases from 0.415 m/s to a maximum of approximately 0.45 m/s above the stadium (an 8% increase). A significant increase also occurs around the sides of the stadium. A large, separated flow region exists in the wake of the stadium, where flow generally tends to move upwards from ground level and against the direction of bulk flow near the leeward side of the stadium. This region is especially prominent in the 45 degree orientation, due to the roof support columns which widen the stadium's exterior profile with respect to incoming flow and cause the wake to be asymmetric.

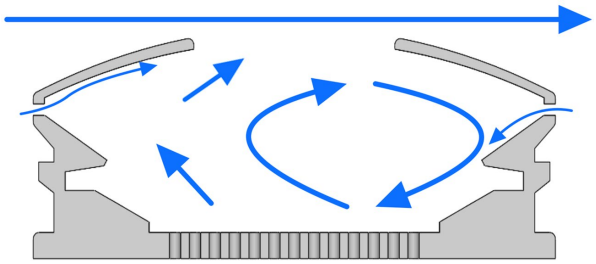

Figure 6. Side profile of the stadium with arrows to illustrate key flow mechanisms and directions at centerplane.

The interior of the stadium is largely shielded from bulk flow in both orientations; however, several porous features enable an interaction between internal and external flow. Near ground level, windward facing tunnels provide the primary means of inflow as impinging bulk flow creates a high pressure region at the front of the stadium. In the 0 degree orientation, support columns obstruct flow near the windward tunnel entrances, although flow into the stadium persists. In the 45 degree orientation, fast-moving flow enters the stadium via a tunnel aligned closely with the bulk flow direction. Towards the top of the stadium, roof level ventilation gaps provide another primary means of inflow. Flow accelerates through a ventilation gap oriented directly upstream in the 0 degree case, and in the 45 degree case, two ventilation gaps provide exposure to fast moving flow from the windward direction.

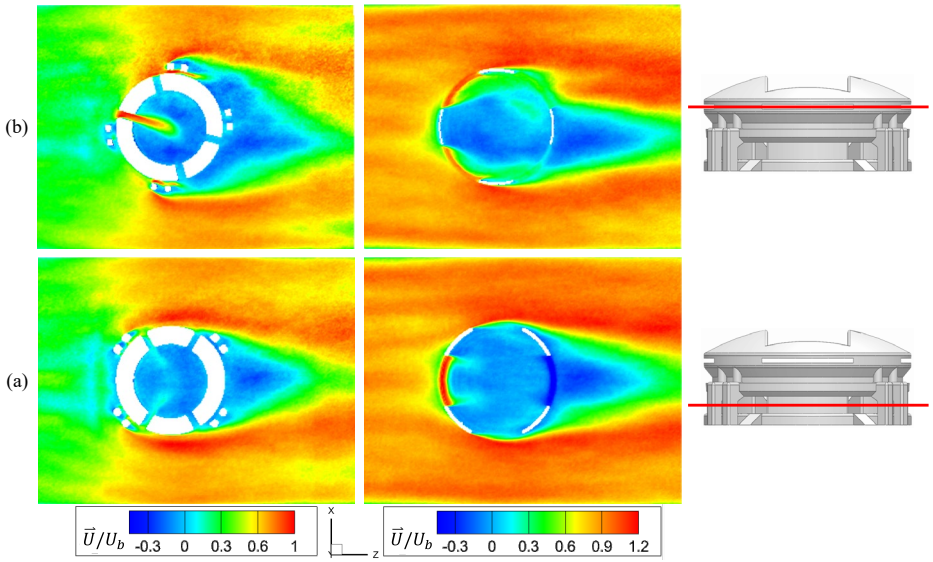

Figure 7. Contour planes of streamwise velocity normalized by bulk velocity located at the horizontal midplane of the tunnels (left) and the midplane of the roof level ventilation gaps (right) for the two stadium orientations: 0 degrees (a) and 45 degrees (b). Red lines on the geometry thumbnails indicate plane locations.

Figure 8 provides quantitative insight into the amount of flow moving in or out of the stadium through the tunnels and roof level ventilation gaps. The flow could not be directly integrated due to partial volume effects. Instead, velocities were obtained along the length of the tunnel centerlines and near the center of the ventilation gaps. The plots indicate that for the 0 degree orientation, flow enters the stadium through leeward openings in addition to the windward openings. In fact, flow into the stadium through the leeward tunnels (tunnels 1 and 4) is approximately one quarter of flow through the windward tunnels (tunnels 2 and 3). Flow through tunnels 2 and 3 is likely impeded by the small separation regions created by the nearby roof support columns (c.f. Fig. 7). Flow also enters the stadium through the leeward ventilation gap (gap 1). The velocity of this flow is over one third of the velocity of flow through the windward gap, which is significant given that the windward gap is directly exposed to freestream flow. Inflows on the leeward side in this orientation occur due to a pressure differential that is created by partial pressure recovery in the stadium wake and low pressure above the stadium roof.

Flow through the leeward tunnels (tunnels 1 and 2) in the 45 degree orientation is more complex. Recirculation within tunnel 1 (the most leeward tunnel) causes flow on the bottom half of the tunnel to move towards the stadium exterior, while flow on the top half of the tunnel moves towards the interior. The large jet created by tunnel 3, which faces directly upstream, likely reduces the interior-exterior pressure difference across tunnel 1, preventing flow in tunnel 1 from preferring a global direction. Inflow through tunnel 4, on the other hand, is not much larger than inflow through the leeward tunnels in the 0 degree case. The windward ventilation gaps (gaps 3 and 4) in the 45 degree case each provide a comparable inflow to the windward gap in the 0 degree case, while gaps 1 and 2 enable more outflow than any gap in the 0 degree case. These results demonstrate that ventilation through stadium openings is strongly influenced by changes in wind angle. Flow through some openings experiences not only a change in magnitude, but also a reversal of direction, as is the case for the leeward tunnels and roof level gap in the 0 degree case.

The final and most substantial means of ventilation is the opening in the stadium roof. For both orientations, the roof opening is the primary means by which flow exits the stadium. The 45-degree opening is angled with respect to the

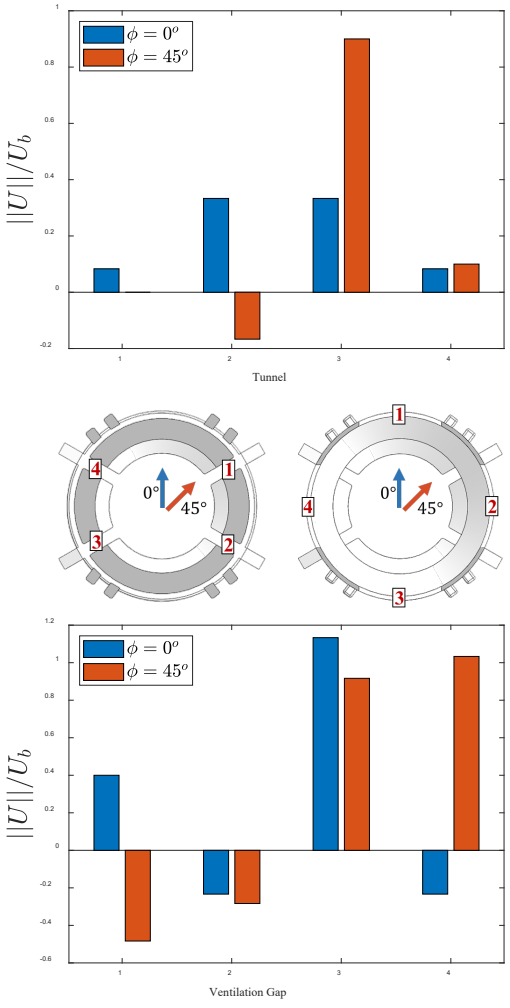

Figure 8. Bar graphs depicting characteristic velocity magnitudes at the centerlines of the tunnels and roof level ventilation gaps for both stadium orientations: 0 degrees (blue) and 45 degrees (red). Flow into the stadium is given by positive values, while flow out is given by negative values. Labels on the geometry thumbnails indicate the locations that correspond with the numbers on the x-axes of the charts. The arrows indicate the freestream flow direction for each stadium orientation.

streamwise flow direction, and as result, a segment of its leeward edge is higher than the corresponding segment of its windward edge. This difference in heights causes some freestream flow to also be directed into the stadium through the 45-degree opening. Flow through the roof in the 0 degree orientation, on the other hand, is almost exclusively exiting the stadium, balancing flow through the tunnel and slot openings.

Scalar Dispersion Analysis

Concentration data are analyzed for the 0 degree orientation. Figure 9 displays isosurfaces at three different concentrations in order to demonstrate general features of the contaminant plume. After injection, contaminant fills the entirety of the stadium, with the highest concentrations residing in the windward half of the stadium. The majority of contaminant exits the stadium via the large rectangular roof opening. Concentrations in the stadium wake are relatively low, being almost entirely below 10%, and the plume approaches the measurement noise floor by the time it reaches the downstream end of the test section. This is an indicator that turbulent mixing is highly effective in the downstream regions of the test section. High concentrations within the stadium relative to the wake suggest that contaminant residence times within the stadium are significant.

While a small amount of contaminant can be seen exiting the stadium via the side roof ventilation gaps, there is no transport out of the leeward ventilation gap. Interestingly, there is also little evidence of contaminant exiting via the tunnels. This is consistent with the characteristic velocities shown in Fig. 8, which demonstrate that all four tunnels in the 0 degree case and the leeward ventilation gap experience inflow. Contaminant therefore exits the stadium almost exclusively through the roof opening, which contributes to the elevated nature of the downstream plume. These observations demonstrate the influence of porous feature ventilation characteristics on the spatial distribution of the downstream plume.

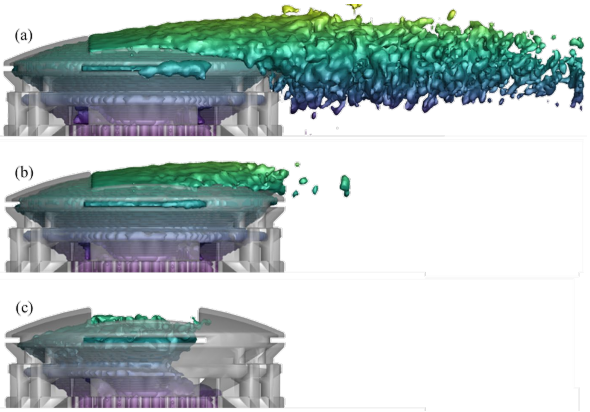

Figure 9. Concentration isosurfaces for C=0.05 (a), C=0.1 (b), C=0.3 (c), with flow moving from left to right. Isosurfaces are colored by height.

The velocity field provides insight into many features of the concentration field. Figure 10 depicts contours of streamwise velocity and concentration at the horizontal midplane of the tunnels. Contaminant near the interior ends of the windward tunnels is diluted by incoming flow. There is also little contaminant within the leeward tunnels because flow moves into the stadium through these tunnels as well. These findings agree with the data shown in Fig. 8.

Figure 11 depicts contours of streamwise velocity and concentration on the vertically orientated stadium centerplane. In general, much of the flow within the lower portion of the stadium moves against the direction of external flow, while closer to the roof, flow moves in the direction of external flow (see also Fig. 6). The effects of this internal recirculation cause the windward side of the stadium cavity to experience the highest levels of contamination. Flow entering the stadium through the ventilation gap on the windward face does little to prevent contamination of the stands, and instead attaches to the bottom surface of the roof overhang. This is consistent with general behavior of wall jets and could also be due to the direction of recirculating flow within the stadium. Flow also enters the stadium through the ventilation gap on the leeward face of the stadium. In this case, the incoming flow does not attach to the bottom surface of the roof, possibly due to the smaller inflow velocity compared to the strength of recirculation within the stadium, and instead, it dilutes some contamination over the second level stands. The velocity and concentration results indicate that recirculation within the stadium is strong enough to influence both the internal concentration field and ventilating flows.

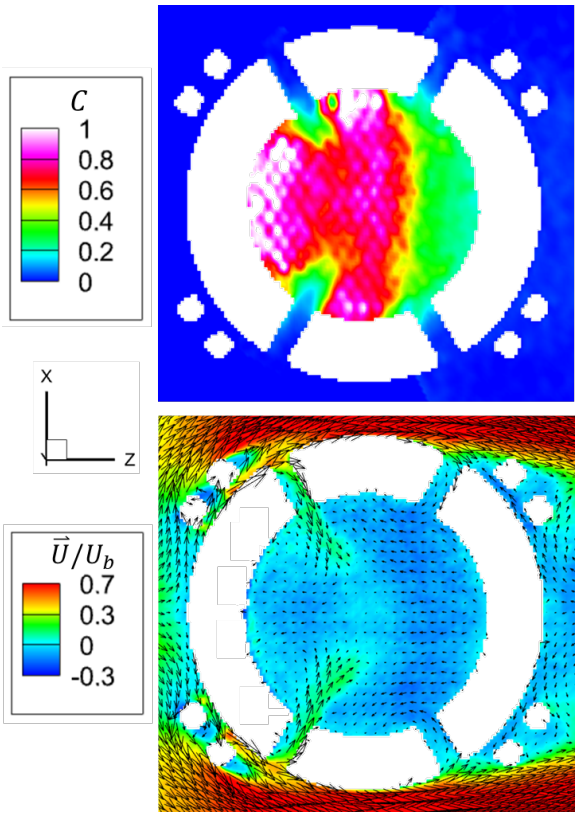

Figure 10. Contour planes located at the midplane of the tunnels, colored by concentration (top) and streamwise velocity (bottom) with velocity vectors displayed.

CONCLUSIONS

MRI techniques were applied to the measurement of flow and scalar dispersion within a stadium, yielding three-dimensional velocity and concentration fields. Velocity measurements were obtained for two orientations of the

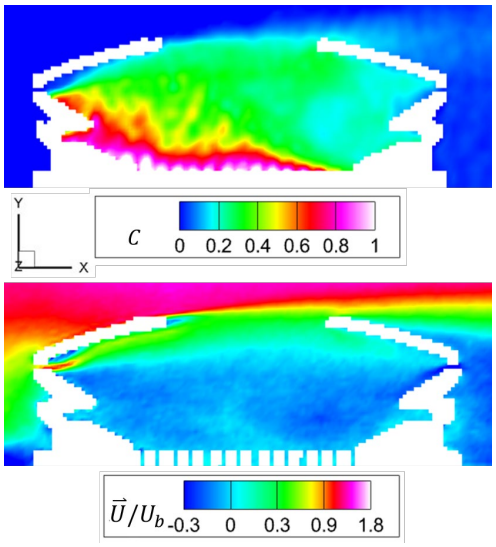

Figure 11. Vertical contour planes located at the centerplane of the stadium, colored by concentration (top) and streamwise velocity (bottom).

stadium relative to the freestream flow direction. The data demonstrate significant differences in ventilation characteristics between the two orientations. In the 45 degree orientation, more openings are exposed to fast moving flow on the windward side of the stadium. This enables strong inflows on that side, while openings on the leeward side enable outflows. The 0 degree orientation experiences inflows through the windward side as well, but also demonstrates that changes in orientation can cause ventilating flows to reverse direction: low pressure above the stadium and partial pressure recovery in the wake foster inflow through leeward tunnels and roof level gaps. Concentration measurements obtained for the 0 degree orientation demonstrate that this phenomenon has an important influence on dispersion, as contaminant exits the stadium almost exclusively through the roof and creates an elevated downstream plume. These results suggest that for natural ventilation design, it is important to consider the placement of openings with respect to external flow features and wind directions.

Ultimately, the three-dimensionality and spatial variability of both the velocity and concentration fields suggest the importance and utility of the detailed MRI datasets for model validation efforts. Future work will therefore apply the data to comparisons with CFD simulations that employ boundary conditions from the experiments. These comparisons can be enhanced with additional quantitative analysis of the ventilation characteristics of the stadium (e.g., using scalar flux calculations). Subsequent MRI experiments can also be performed to collect velocity and concentration data for different wind angles, and a transient release can be explored using phase-locked imaging.

REFERENCES

Banko, A. J., et al., 2020, "An improved three-dimensional concentration measurement technique using magnetic resonance imaging," *Exp. Fluids*, vol. 61, no. 2, p. 53.

Benson, M. et al., 2019, "Detailed magnetic resonance imaging measurements of a contaminant dispersed in an Oklahoma City model," *Atmos. Environ.*, p. 117129.

Blocken, B., 2015, "Computational Fluid Dynamics for urban physics: Importance, scales, possibilities, limitations and ten tips and tricks towards accurate and reliable simulations," *Build. Environ.*, vol. 91, p. 219-245.

Britter, R. E., and Hanna, S. R., 2003, "Flow and Dispersion in Urban Areas," *Annual Rev. Fluid Mech.,* vol. 35, p. 469-496.

Brown, A. L. et al., 2020, " An urban dispersion inspired scenario for CFD model validation," *Fire Safety Journal,* vol. 120, p. 103130.

Caciolo, M. et al., 2011, " Full scale experimental study of single-sided ventilation: Analysis of stack and wind effects," *Energy and Buildings,* vol. 43, no. 7, p. 1765-1773.

Elkins, C. J., and Alley, M. T., 2007, "Magnetic resonance velocimetry: applications of MRI in the measurement of fluid motion," *Exp. Fluids*, vol. 43, no. 6, pp. 823–858.

Homan, T. A. et al., 2021, " Magnetic Resonance Imaging measurements of scalar dispersion for a scaled urban transient release," *Build. Environ.,* vol. 205, p. 108163.

Jiang, Y. et al., 2003, "Natural ventilation in buildings: measurement in a wind tunnel and numerical simulation with large-eddy simulation," *Journal of Wind Eng. and Industrial Aerodynamics*, vol. 91, no. 3, p. 331-353.

Lateb, M. et al., 2016, "On the use of numerical modelling for near-field pollutant dispersion in urban environments − A review," *Environ. Pollut.,* vol. 208, p. 271-283.

Lien, FS. and Yee, E., 2004, "Numerical Modelling of the Turbulent Flow Developing Within and Over a 3-D Building Array, Part I: A High-Resolution Reynolds-Averaged Navier—Stokes Approach," *Boundary-Layer Meteorology,* vol. 112, p. 427–466.

Lo, L. J., and Novoselac, A., 2012, "Cross ventilation with small openings: Measurements in a multi-zone test building," *Build. Environ.,* vol. 57, p. 377-386.

Ohba, M. et al., 2001, "Study on airflow characteristics inside and outside a cross-ventilation model, and ventilation flow rates using wind tunnel experiments," *Journal of Wind Eng. and Industrial Aerodynamics,* vol. 89, p. 1513-1524.

Owkes, M. et al., 2020, "Three-dimensional velocity and concentration measurements and simulations of a scaled Jack Rabbit II mock urban array," *Atmos. Environ.,* vol. 233, p. 117520.

Remion, G. et al., 2019, "Review of tracer gas-based methods for the characterization of natural ventilation performance: Comparative analysis of their accuracy," *Build. Environ.,* vol. 160, p. 106180.

Shankar, P. N., and Deshpande, M., 2000, "Fluid mechanics in the driven cavity," *Annual Rev. Fluid Mech.*, vol. 32, p. 93-136.

Shim, G. et al., 2019, "3D MRI measurements of the effects of wind direction on flow characteristics and contaminant dispersion in a model urban canopy," *Environ. Fluid Mech.,* vol. 19., p. 851-878.

Van Hooff, T., and Blocken, B., 2010, "On the effect of wind direction and urban surroundings on natural ventilation of a large semi-enclosed stadium," *Comput. Fluids*, vol. 39, no. 7, pp. 1146–1155.

Van Hooff, T., and Blocken, B., 2013, "CFD evaluation of natural ventilation of indoor environments by the concentration decay method: CO2 gas dispersion from a semi-enclosed stadium," *Build Environ*, vol. 61, p. 1–17.